Delft University of Technology

Bachelor Applied Mathematics and Physics
Bachelor End Project

Modelling tidal winds in coastal areas

Author:
Joppe van Soest 5176352

Responsible supervisors:
Prof.dr.ir. Chris Kleijn and Prof.dr.ir. Martin Verlaan

TU Delft
Faculty of Electrical Engineering, Mathematics & Computer Science
Faculty of Applied Sciences
July 16, 2024 Delft

Abstract

To optimally use wind farms, thorough understanding of wind patterns is needed. Recently, a lot of attention in the scientific community is turned to the Current FeedBack effect, where oceanic currents influence the atmosphere above. It has been shown that this also applies to tidal currents in the English Channel where the induced tidal winds have an amplitude of one-third of the underlying current. In this report focus is moved to the Dutch coast. Using a numerical integration model of a vertical grid, the horizontal wind speeds above a small area of the Dutch coast are modelled. The model is based on the 1-dimensional Navier-Stokes equations in combination with Prandtl's mixing length model to account for turbulence. The horizontal wind speeds are found to reach up to one-fourth of the amplitude of the tidal currents at a height of $z = 10m$ above the sea surface and $1/20$ at $z = 50m$. This is similar to what was found in earlier research, but a lot of assumptions were made in this model. Therefore, further research could focus on addressing some of these assumptions such that the understanding of tidal induced wind velocities can be even better understood.

Contents

List of Symbols

Variable	Symbol	Units
Wind speed	u	$\frac{m}{s}$
Height	z	m
Time	t	s
Kinematic Viscosity	ν	$\frac{m^2}{s}$
Eddy viscosity	ν_t	$\frac{m^2}{s}$
Mixing length	l_m	m
Von Kármán constant	κ	$-$
Shear stress	τ	$\frac{kg}{ms^2}$
Density	ρ	$\frac{kg}{m^3}$
Amplitude	A, B	$\frac{m}{s}$
Absolute tolerance	$atol$	$-$
Relative Tolerance	$rtol$	$-$
Period	T	s
Constant	C	$-$

Introduction

In the fight against climate change, the energy transition plays a crucial role. To reduce CO_2 emissions and conserve our resources, we need clean and renewable energy. To achieve the EU goal of being climate neutral by 2050 [6], the Netherlands is investing in wind power. Currently, almost a quarter of the electricity demand is met by wind farms, with 37% of that coming from offshore installations [3]. By 2030, the Dutch government aims to make offshore wind energy the largest source of electricity in the country [7]. This means many new wind farms will be installed in the coming years. To optimally use these wind farms, understanding wind patterns along the coast is essential for improving weather forecasting.

Weather forecasting is a very complex process. As much data as possible is gathered, which is then put in mathematical models that simulate the atmospheric behaviour. Data assimilation techniques combine these models with observations to come to the best forecast[11]. As the atmosphere is very chaotic and complex, using the right initial conditions and boundary conditions, such as the sea, is of utmost importance. Recently, air-sea interactions at the atmospheric mesoscale(scales of $10 - 100$ km and $10 - 100$ days) have gained increasing interest from the scientific community[4][17]. Foremost, this applies to the Current FeedBack(CFB) effect, in which the surface currents lose energy to the atmosphere above[12]. This way the atmosphere acts as an energy sink for the sea[14]. The other way around, the sea acts as an energy source for overlying winds. Now, the sea-atmosphere interaction cannot only be seen as a one-way interaction, but as an exchange of energy in both directions.

However, the effect this has on tidal currents and induced tidal winds has not received as much attention. Renault and Marchesiello addressed this and investigated the tidal induced winds in the English Channel. They found that these tidal winds at $10m$ high can reach speeds approximately one-third of the underlying tidal currents [13]. To this day though, tidal currents are not yet used as part of the surface boundary condition in modern forecasting models[5].

In this report we will focus on an area at the Dutch coast. We will look into the influence of tidal currents on wind speeds above the coast of the Netherlands. We will numerically simulate the surface layer using the 1-dimensional Navier-Stokes equations in combination with a relatively simple turbulence model, Prandtl's mixing length model. We will first run our simulations assuming the atmosphere is laminar because we can solve this analytically as well. This way we can check whether our numerical integration is validated or not. Afterwards we will run some simulations with turbulent flow on the Dutch coast to see if we get a tidal induced wind of one-third the underlying tidal current as well.

This report first introduces the atmospheric boundary layer and explores the relevant physics in the next chapter, introducing the mixing length model used to simulate turbulent air flow as well. It also elaborates on the analytical solutions to the problem. Following this chapter, the results will be presented. The report concludes with a discussion and a conclusion.

Model

2.1 Atmospheric boundary layer

In the following section we will describe the atmospheric boundary layer and the analysis of turbulent motion inside it using [9]. The atmospheric boundary layer is the lowest layer of our atmosphere. It is highly influenced by the interaction with the Earths' surface and reacts rapidly to surface changes such as friction, solar heating and evaporation. Therefore, the boundary layer is highly turbulent. Because the boundary layer is connected to the surface, it is influenced a lot by the diurnal cycle of surface heating through the day, and cooling through the night. This means that during the day the atmospheric boundary layer is very unstable because the air close to the surface is heated which results in an unstable boundary layer. To determine wind speeds we have to solve the Navier Stokes equations, however in most turbulent flow these cannot be solved analytically. Therefore, we have to turn to numerically solving the equations. Turbulent flow is characterised by irregular quasi-random motions that span a continuous spectrum of spatial and temporal scales. These are in most cases impossible to simulate numerically on the smallest scales, therefore we are looking at the time averaged momentum equations. We assume that the velocity field is characterised by a slowly varying mean field $\overline{u}$ and rapidly changing turbulent motions u' and v'. These turbulent motions disappear if we time average, however their covariance typically does not. We are considering a neutrally stratified atmosphere, such that we can neglect buoyancy influences.

Therefore turbulence models focus on approximating the behaviour of these covariances. Away from horizontal inhomogeneities we can assume that these turbulent motions are horizontally homogeneous so we only have to consider vertical differentiation.

$$\frac{\partial u}{\partial t} = \frac{\partial}{\partial z}(\nu \frac{\partial u}{\partial z} - \overline{u'v'}) \tag{2.1}$$

In our case we will look at the lowest part of the atmospheric boundary layer, the surface layer which spans typically 10%, so on average approximately 100 m. In this surface layer we can approximate the wind to be horizontal, parallel to the surface of the sea. The surface layer is maintained entirely by vertical momentum transfer by turbulent eddies. Therefore in our model, we will simplify the problem to a vertical grid from the sea surface z_0 to the top of the surface layer z_{top} where we determine the wind speeds using boundary conditions at the surface and at the top of our surface layer.

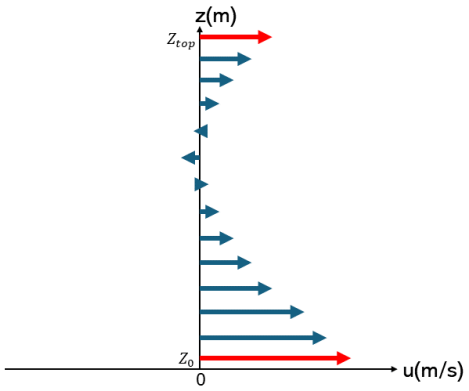

Figure 2.1: Representation of the situation in which we have brought it down to a vertical grid in which we numerically determine the wind speeds using two boundary conditions indicated by the bottom and top red arrows at z_0 and z_{top}. The blue arrows indicate the numerically determined wind speeds at the different grid points.

2.2 Prandtl's mixing length model

We will describe the mixing length model analogous to [9] and [16]. Prandtl's mixing length model is one of the oldest and simplest models for the $\overline{u'v'}$ covariance term in equation 2.1. In neutrally stratified boundary layers, the wind speeds varies significantly with height. In the surface layer, in order to analyse the turbulent flow use is made of the eddy viscosity concept. It builds on the Boussinesq's eddy viscosity concept, which characterises the turbulent flow by an eddy viscosity similar to molecular viscosity, however eddy viscosity depends on the flow itself.

$$\overline{u'v'} = -\nu_t \frac{\partial u}{\partial z} \tag{2.2}$$

The mixing length model, introduced by Ludwig Prandtl, assumes that a parcel of fluid is vertically displaced over a characteristic length l_m carrying the mean properties of its original level before mixing with its surroundings. Therefore the eddy viscosity is proportional to the product of this characteristic length and a velocity scale.

$$\nu_t \propto \hat{V} L \tag{2.3}$$

Prandtl proposed that the velocity component is equal to the mean velocity gradient times the mixing length l_m, so $\hat{V} = l_m \left|\frac{\partial u}{\partial z}\right|$. This mixing length l_m is also the characteristic length L. This leads to

$$\nu_t = l_m^2 \left|\frac{\partial u}{\partial z}\right| \tag{2.4}$$

In the surface layer this length scale is linearly dependent on the distance from the surface, the height z, and proportional to the Von Kármán constant κ. So $l_m = \kappa z$ which results in

$$\frac{\partial u}{\partial t} = \frac{\partial}{\partial z}[(\nu + \kappa^2 z^2 \left|\frac{\partial u}{\partial z}\right|)\frac{\partial u}{\partial z}] \tag{2.5}$$

Equation 2.5 can be divided into two parts, one where the time derivative of the wind speed is a function of the spatial derivative of the stress and a function for the stress

$$\frac{\partial u}{\partial t} = \frac{1}{\rho}\frac{\partial \tau}{\partial z} \tag{2.6}$$

$$\tau = \rho(\nu + \kappa^2 z^2 \left|\frac{\partial u}{\partial z}\right|)\frac{\partial u}{\partial z} \tag{2.7}$$

2.3 Numerical integration

Equation 2.5 with appropriate boundary and initial conditions cannot, generally, be solved analytically. Therefore, we will solve these equations numerically. For the coding in this report we use Python. For the numerical integration we use *integrate.solve_ivp*, this is a numerical solver from the *scipy* library. It can solve a system of ordinary differential equations. This solver can use different methods to come to a solution but in this report the Radau method has been used. This is an implicit Runge-Kutta method of the Radau IIA family of order 5 [8]. It was found that this was the most reliable and quickest integration method. The solution is influenced by the number and distribution of grid points we put in and by the tolerances *atol* and *rtol*, the relative and absolute tolerances respectively, which determine the time step size. The function itself calculates an estimate error with a third-order embedded formula and it keeps this error under $atol + rtol|y|$ where y is the solution at the desired point. By decreasing *atol* and *rtol* we can increase the accuracy.

2.3.1 Grid

In our study we will make use of two kinds of grids. First, we will disregard turbulence and therefore equation 2.5 becomes linear, calling for a linear grid. When we later do consider turbulence, this calls for a logarithmic grid, due to the z^2 term in equation 2.5. In both cases we will use a staggered grid, where we alternate between points where we calculate the stress and where we calculate wind speed. We first set all the z_τ, the points where we want to know the stress. Then a second grid is determined for the heights for which we want to determine u, these grid points lie exactly in between two consecutive z_τ grid points. So

$$z_{u,i} = (z_{\tau,i} + z_{\tau,i+1})/2 \tag{2.8}$$

The stress points for the linear grid are determined by

$$z_{\tau,i} = z_0 + (\frac{1}{2} + i)\frac{z_{top} - z_0}{n} \tag{2.9}$$

where we have n grid points with i running from 0 to $n-1$. For the logarithmic grid, we use

$$z_{\tau,i} = z_{top}(\frac{z_{top}}{z_o})^{\frac{i-n+1}{n-1}} \tag{2.10}$$

where again we have n grid points with i running from 0 to $n-1$.

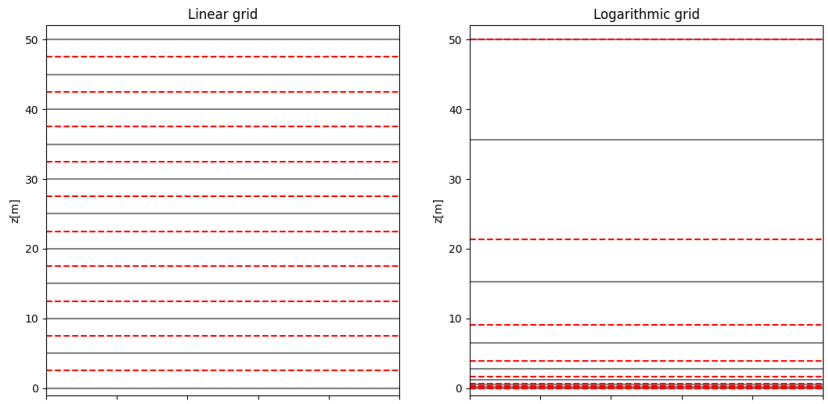

Figure 2.2: Representation of the grid points. On the left we have a linear grid, on the right a logarithmic grid. The gray lines represents the z_u points, whereas the dashed red lines represent the z_τ points.

We also begin with a certain initial condition $u(z, t = 0)$.

2.3.2 System of ODE's

Every iteration the solver takes, it first determines all the stresses τ

$$\tau_i = (\nu + \kappa^2 z_{tau,i}^2 \left| \frac{u_{i+1} - u_i}{z_{u,i+1} - z_{u,i}} \right|) \frac{u_{i+1} - u_i}{z_{u,i+1} - z_{u,i}} \tag{2.11}$$

where u_i are the computed wind speeds at the last known time. We assume ρ to be constant so therefore we can omit it from equations 2.6 and 2.7. With these stresses we can determine the change in wind speed for every grid point z_u

$$\frac{\partial u_i}{\partial t} = \frac{\tau_i - \tau_{i-1}}{z_{\tau,i} - z_{\tau,i-1}} \tag{2.12}$$

with these $\frac{\partial u_i}{\partial t}$ we can determine the new u_i.

2.4 Considered Flows

To first validate our model, we turn to analytically solvable situations. We first consider laminar flow because we can solve it for transient cases as well. We start with constant velocity at one boundary and work our way up to periodically oscillating velocity at both boundaries. Thereafter we will turn to turbulent flow, where we can still determine the equilibrium solution for constant velocity at both boundaries. We will conclude by using real data from the Dutch coast to simulate the behaviour of the tide induced wind speeds

- Laminar flow
  - Constant velocity bottom boundary
  - Periodically oscillating velocity at bottom boundary
  - Periodically oscillating velocity at both boundaries
- Turbulent flow
  - Constant velocity at top and bottom boundaries
  - Periodically oscillating flow at bottom boundary
  - Boundary conditions taken from real measurements

2.4.1 Laminar flow

When laminar flow is considered we can set $\kappa = 0$. This reduces equation 2.5 to

$$\frac{\partial u}{\partial t} = \nu \frac{\partial^2 u}{\partial z^2} \tag{2.13}$$

Constant velocity at top and bottom boundaries

When considering constant velocities at the boundaries, we start from an initial condition where velocity is 0 everywhere. It can be seen that only the difference between the top and bottom boundary matters, so we set the top boundary to 0 as well. We get boundary conditions and initial condition

$$\begin{aligned} u(z_0, t) &= A \\ u(z_{top}, t) &= 0 \\ u(z, 0) &= 0 \end{aligned} \tag{2.14}$$

using these boundary conditions we can solve 2.13 using separation of variables, see Appendix A. Which leads to the solution

$$u(z,t) = A\frac{z_{top}-z}{z_{top}-z_0} - \sum_{n=1}^{\infty}\frac{2A}{n\pi}sin(n\pi\frac{z-z_0}{z_{top}-z_0})e^{-\nu(\frac{n\pi}{z_{top}-z_0})^2 t} \tag{2.15}$$

This solution cannot be calculated exactly due to the infinite sum but if we take n high enough the solution will be a good enough approximation. Note that for $t \to \infty$ the solution will converge to the first term on the right-hand side of the equation. The term with $n = 1$ will vanish the slowest with a time scale of $\frac{(z_{top}-z_0)^2}{\pi^2\nu}$.

Periodically oscillating velocity at bottom boundary

For periodically oscillating flow at the bottom boundary, the exact solution is a lot more difficult to determine. Therefore, we will only look at the boundary conditions and not consider a particular initial condition. After computing the exact solution to the boundary conditions, we can set the initial condition such that it already satisfies the solution to the boundary conditions. It can be argued that the effect of the initial condition will disappear over time, such that we are computing a limiting periodic solution. This leads to boundary conditions

$$\begin{aligned} u(z_0,t) &= Acos(\omega t) \\ u(z_{top},t) &= 0 \end{aligned} \tag{2.16}$$

The solution to this problem is the following, see appendix A for a detailed derivation

$$u(z,t) = \frac{A}{2}(e^{i\omega t}\frac{sin((z_{top}-z)(1+i)\sqrt{\frac{\omega}{2\nu}})}{sin((z_{top}-z_0)(1+i)\sqrt{\frac{\omega}{2\nu}})} + e^{-i\omega t}\frac{sinh((z_{top}-z)(1+i)\sqrt{\frac{\omega}{2\nu}})}{sinh((z_{top}-z_0)(1+i)\sqrt{\frac{\omega}{2\nu}})}) \tag{2.17}$$

Although it seems as if this solution is complex, it can be seen that this is an addition of a complex function and it's complex conjugate, which is a real function. Note that if $\frac{\Delta z^2\omega}{2\nu} = \frac{\Delta z^2\pi}{\nu T} = C$ with C a constant, the solution remains mathematically similar, where $\Delta z = z_{top} - z_0$. This is equivalent to the case with a constant boundary, where if $\frac{\Delta z^2}{\pi^2\nu T} = C$, the solution remains mathematically similar.

Periodically oscillating flow at both boundaries

If we consider a periodically oscillating flow at both boundaries we have the following boundary conditions

$$\begin{aligned} u(z_0,t) &= Acos(\omega t) \\ u(z_{top},t) &= Bcos(\psi t + \phi) \end{aligned} \tag{2.18}$$

Let u' and u'' such that they both satisfy the partial differential equation and the boundary condition at z_0 and z_{top} respectively. For the other boundary condition we set them equal to 0, so

$$u'_t = u'_{zz} \qquad u''_t = u''_{zz} \tag{2.19}$$

$$u'(z_0,t) = Acos(\omega t) \qquad u''(z_0,t) = 0 \tag{2.20}$$

$$u'(z_{top},t) = 0 \qquad u''(z_{top},t) = Bcos(\psi t + \phi) \tag{2.21}$$

Now we can see that $u = u' + u''$. The solution for u' we already computed in the last section. For u'' we only have to account for the extra phase factor ϕ. However we can just take this in the exponent with the ωt term. So the solution is

$$\begin{aligned} u(z,t) = \frac{A}{2}(e^{i\omega t}\frac{sin((z_{top}-z)(1+i)\sqrt{\frac{\omega}{2\nu}})}{sin((z_{top}-z_0)(1+i)\sqrt{\frac{\omega}{2\nu}})} + e^{-i\omega t}\frac{sinh((z_{top}-z)(1+i)\sqrt{\frac{\omega}{2\nu}})}{sinh((z_{top}-z_0)(1+i)\sqrt{\frac{\omega}{2\nu}})}) \\ + \frac{B}{2}(e^{i\psi t+\phi}\frac{sin((z-z_0)(1+i)\sqrt{\frac{\psi}{2\nu}})}{sin((z_{top}-z_0)(1+i)\sqrt{\frac{\psi}{2\nu}})} + e^{-i\psi t-\phi}\frac{sinh((z-z_0)(1+i)\sqrt{\frac{\psi}{2\nu}})}{sinh((z_{top}-z_0)(1+i)\sqrt{\frac{\psi}{2\nu}})}) \end{aligned} \tag{2.22}$$

2.4.2 Turbulent flow

When considering turbulent flow, we cannot set κ to 0. κ is empirically determined to be 0.4. Therefore, for the turbulent flow case, we need to use equation 2.5. Turbulent flow does not reach the surface itself, there is a very small viscuous sublayer and a transition zone to turbulent flow. Therefore it is common to take the bottom boundary a little bit above the surface, for the sea $z_0 = 0.01m$ can be used[13]. This roughness usually relates to wind waves over sea, but it is very small compared to the wave height.

Constant velocity at top and bottom boundaries

We notice that even though the eddy viscosity ν_t depends on u_z and z, mathematically it is still only the difference between the speed at z_0 and z_{top} that matters. So we will again only use one inhomogeneous boundary condition. We note that equation 2.5 is very hard to solve for the transient case. Therefore we will only solve for the steady state solution. We can set the initial speed to 0.

$$\begin{aligned} u(z_0, t) &= A \\ u(z_{top}, t) &= 0 \\ u(z, 0) &= 0 \end{aligned} \tag{2.23}$$

The steady state solution is the following, see appendix A for the derivation.

$$u_{ss}(z) = A\frac{log(\frac{z}{z_{top}})}{log(\frac{z_0}{z_{top}})} \tag{2.24}$$

for all the other cases with turbulent flow we do not have any analytical solutions.

Results

3.1 Laminar flow

Laminar flow is not realistic for the atmospheric boundary layer, however we use it to validate the model because we are still able to compute an analytical solution for it. We therefore do not have to use realistic values, so we set $A = 1$ for all laminar cases. For the laminar cases we will also use a linear grid, as equation 2.13 is linear.

3.1.1 Constant velocity at bottom boundary

For constant velocities at both boundaries, which was found to be analogous to only one boundary with velocity, we cannot compute an exact solution due to the infinite sum in 2.15. However, we can approximate it by taking n large enough. We used $n = 100$ and $\nu = 1\frac{m^2}{s}$ and $\Delta z = 50m$ with 50 evenly spaced grid points such that every grid point is $1m$.

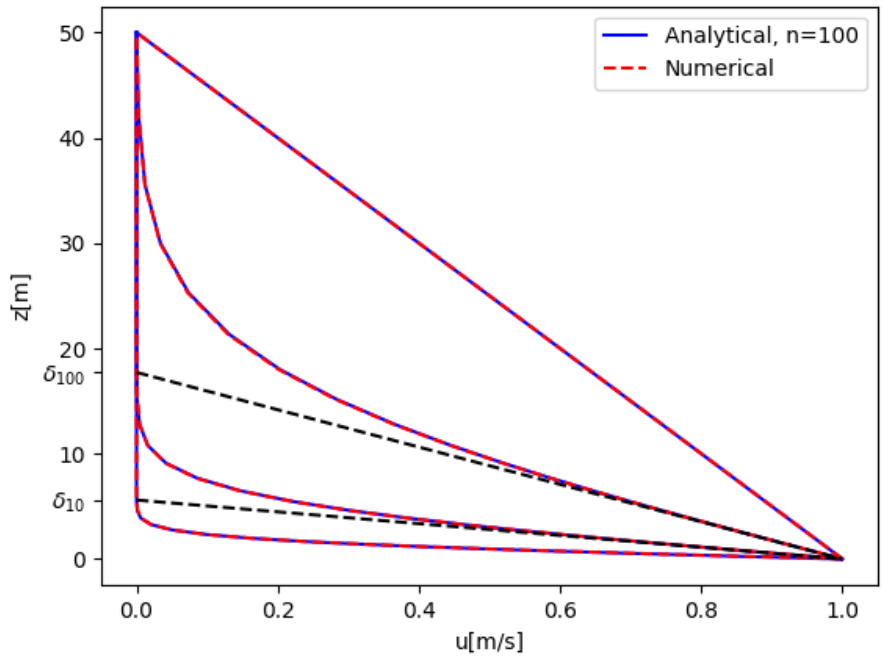

Figure 3.1: Wind speed in $\frac{m}{s}$ plotted against the height z in m for $t = 1, 10, 100, 1000s$. 50 grid points have been used for the numerical solution and the infinite sum in the analytical solution is approximated till $n = 100$. $atol = 10^{-4}$, $rtol = 10^{-5}$. The penetration distance at $t = 10, 100$ is shown by the dashed lines

It can be seen that the numerical solution accurately follows the analytical solution because the dashed line is almost exactly on top of the solid line. If the Fourier number $Fo = \frac{\nu t}{\Delta z^2} < 0.1$ we can use penetration theory to determine the penetration depth $\delta_t = \sqrt{\pi \nu t}$ [1]. For $t = 10s$, $\delta_{10} = 5.6m$

and for $t = 100s$, $\delta_{100} = 17.7m$ with $Fo_{10} = 4 * 10^{-3}$ and $Fo_{100} = 0.04$. If we look at the numerically and analytically derived penetration depth, where the dashed lines end at $u = 0$, these correspond to $5.6m$ for $t = 10s$ and $17.7m$ for $t = 100s$. Exactly what we determined with penetration theory. For $t = 1000s$, $Fo = 0.4 > 0.1$ so we cannot use penetration theory anymore. At $t = 1000s$ the solution seems to have reached the equilibrium solution.

3.1.2 Periodically oscillating velocity at bottom boundary

If we are looking at periodically oscillating velocity, the quantity $\frac{\Delta z^2 \omega}{2\nu} = \frac{\Delta z^2 \pi}{\nu T} = C$ starts to play a role. Therefore we will look at situations where $C = 0.1, 1, 10$. We set the initial condition equal to the analytical solution and then run for 100 periods. This way we still have an analytical solution but mitigate the effect of starting with the perfect solution.

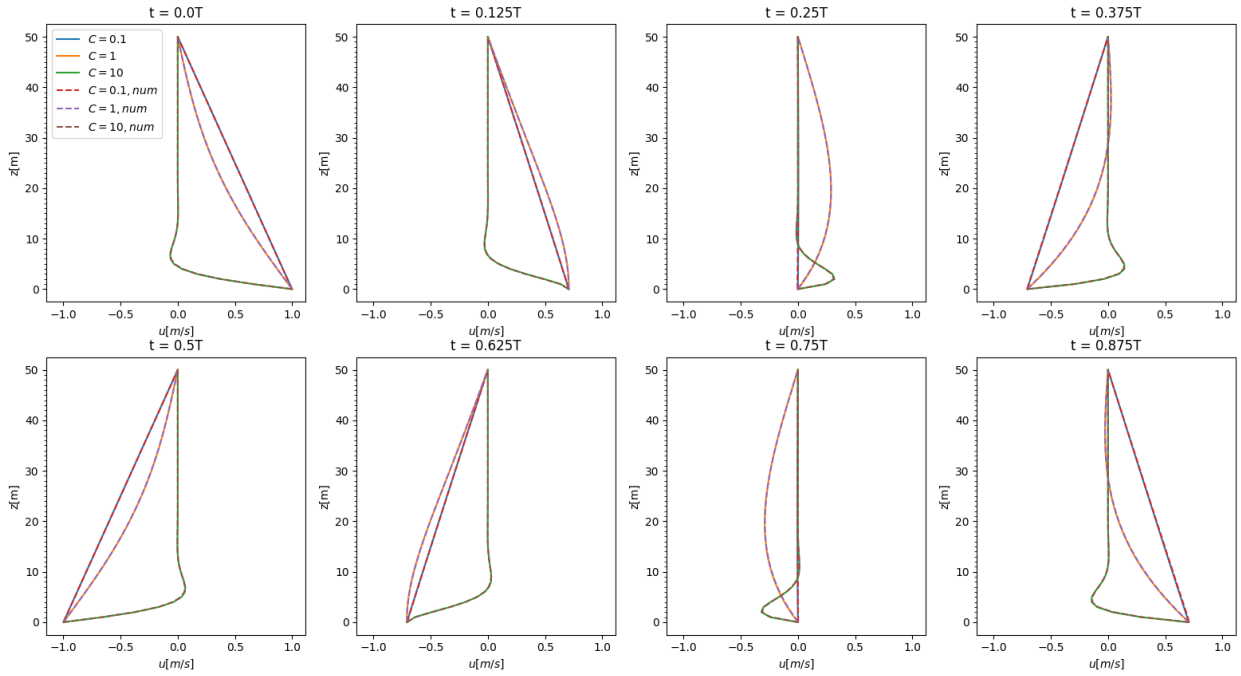

Figure 3.2: Wind speeds in $\frac{m}{s}$ with $C = 0.1, 1, 10$ plotted against the height z in m for 8 evenly spaced times in the $100th$ period. 50 grid points have been used. $atol = 10^{-4}$, $rtol = 10^{-5}$

In this figure we clearly see the periodic behaviour of the different solutions for $C = 0.1, 1, 10$. For $C = 0.1$, $\pi \Delta z^2$ is small compared to νT, so the solution is always almost in its equilibrium position. For $C = 1$, $\pi \Delta z^2$ and νT are equal, so although the boundary condition at z_0 does penetrate the entire altitude, it doesn't reach its equilibrium position. For $C = 10$, $\pi \Delta z^2$ is very large compared to νT and so the boundary condition only influences the bottom part. In the following figure we see the difference even better.

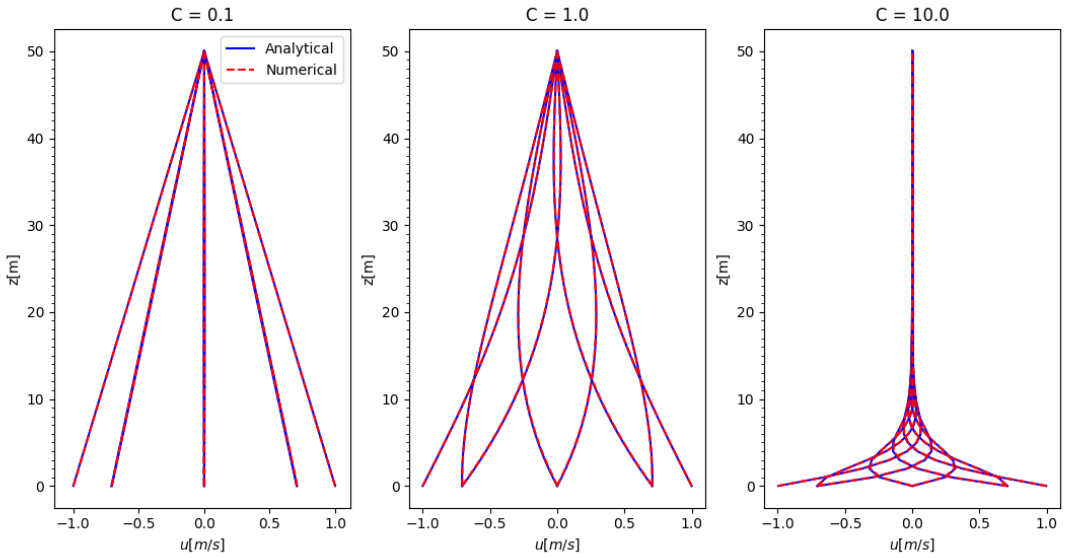

Figure 3.3: The wind speed in $\frac{m}{s}$ plotted against the height z in m for 8 evenly spaced times in the $100th$ period. Plotted for $C = 0.1, 1, 10$ with 100 grid points. For $C = 0.01$ there are also 8 times plotted but 3 are almost exactly on another time t. $atol = 10^{-4}$, $rtol = 10^{-5}$

Again we see in both figures that the numerical solution seems to follow the analytical solution very well.

For this numerically derived solution we analysed the error compared to the analytically determined solution in equation 2.17. We looked at the mean deviation from this analytical solution, so

$$error = \frac{1}{n * N} \sum_{i=0}^{n-1} \sum_{j=0}^{N} \left| u_{i,t_j} - u(z_i, t_j) \right| \tag{3.1}$$

where n is the number of grid points, N number of time steps. $u_{k,t}$ is the numerically determined solution, whereas $u(z_k, t)$ is the analytically computed solution. We controlled the time step using a max_step in the solver.

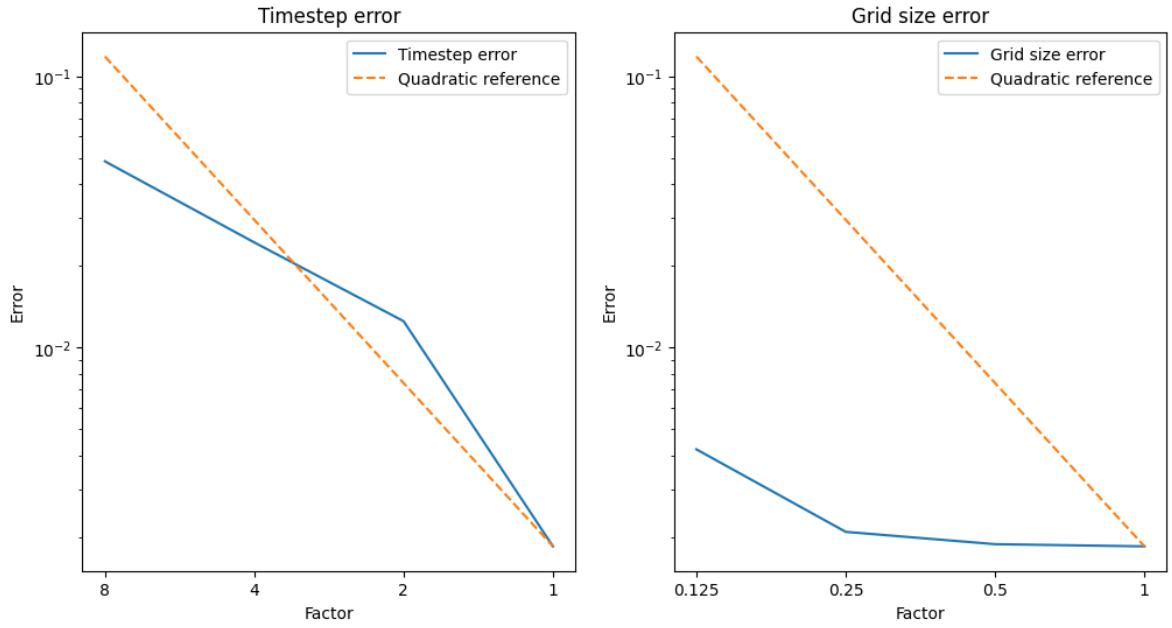

Figure 3.4: The mean error logarithmically plotted for the time step and grid size. The time step was increased by a factor 2, 4 and 8. The grid size was decreased by a factor $\frac{1}{2}$, $\frac{1}{4}$ and $\frac{1}{8}$. In both cases a quadratic relation is plotted as well.

It can be seen that the time step error follows the quadratic relation quite well whereas the grid size error does converge but is quite flat. This could mean that the time step is what mainly determines the error at this stage. We could decrease the time step even more but due to the time it takes to perform a simulation, this was not done.

Periodic flow at both boundaries

For the periodic flow at both boundaries we should note that if we take $A = B$, $\phi = \psi$, $\delta = \pi$ and Δz twice as large, we should get the same solution as with one boundary, now mirrored at $z = 50$.

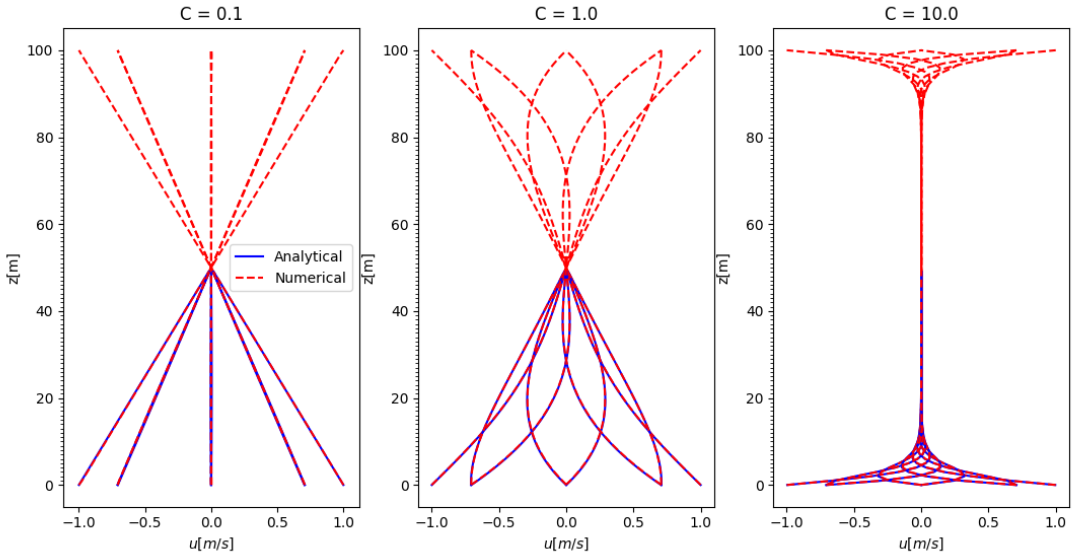

Figure 3.5: Wind speed in $\frac{m}{s}$ plotted against the height z in m for 8 evenly spaced times in the $100th$ period. The analytical solution is computed for a periodic flow at one boundary condition only. Plotted for $C = 0.1, 1, 10$ with 100 grid points. $atol = 10^{-4}$, $rtol = 10^{-5}$

In this situation, the two periods are still the same. The solution should also work for two boundaries that do something completely different. For the next simulation, we used $A = 1\frac{m}{s}$ and $B = 3\frac{m}{s}$, $T_0 = 4300s$ period of the bottom and $T_{top} = 1900s$ period of the top, $\delta = 1$. If we take a weighted average of the periods, we can still approximate a C. So we still use $C = 0.1, 1, 10$ but then compared to total weighted T

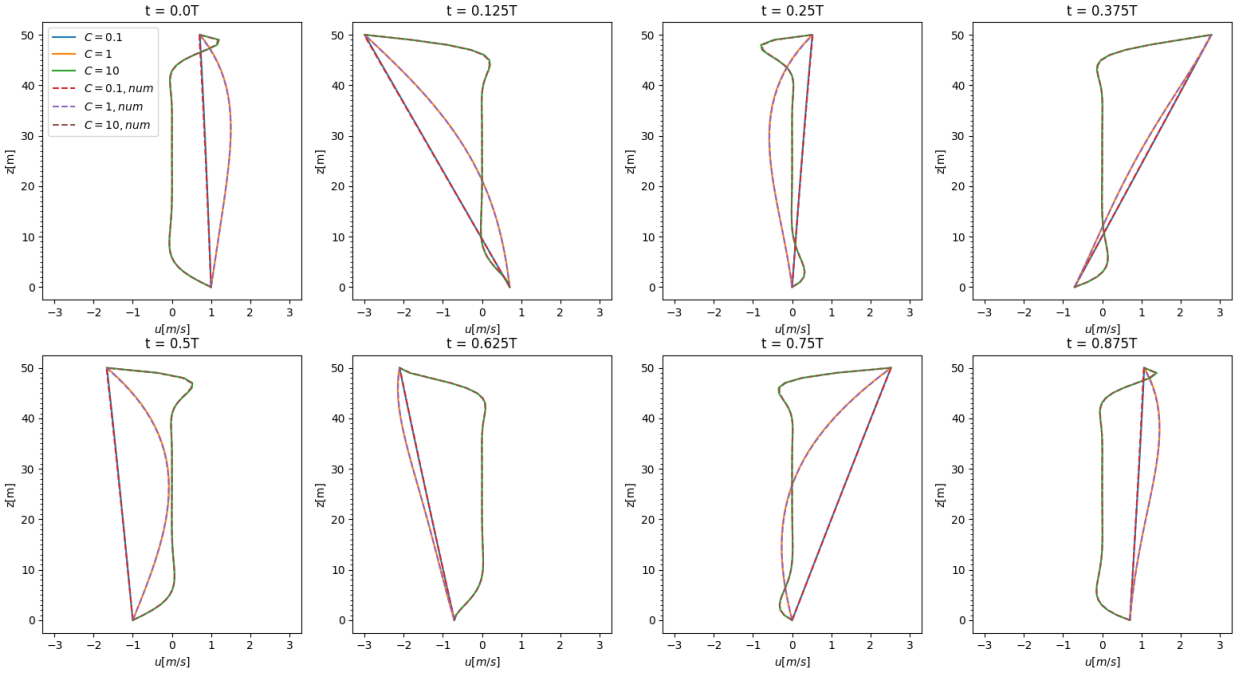

Figure 3.6: Wind speeds in $\frac{m}{s}$ plotted against the height z in m for 8 evenly spaced times in the $100th$ period of the bottom, so $t : [99T_0, 100T_0]$. The top amplitude is 3 times the bottom amplitude and $T_{top} = 1900$, $T_0 = 4300$ with $\delta = 1$. Plotted for $C = 0.1, 1, 10$ with 100 grid points. $atol = 10^{-4}$, $rtol = 10^{-5}$

.

We see that still for periods, amplitudes and phase difference that aren't "nice", the numerical solution still follows the analytical solution. We see as well that with the weighted T, the behaviour for the different values of C is still the same. So for $C = 0.1$, the boundary conditions influence up to $10m$ and for $C = 10$, the solution is almost in equilibrium position.

3.2 Turbulent flow

For turbulent flow $\kappa = 0.4$ and not 0, so equation 2.5 is not linear anymore, $\nu = 1.5 * 10^{-5}\frac{m^2}{s}$. We therefore have to consider whether a linear grid is still preferable or if we should use a logarithmic grid to ensure a better resolution for lower heights. In the Model chapter we already argued that a logarithmic grid would work better in this case.

3.2.1 Constant velocity at bottom boundary

We again only look at the bottom boundary having a velocity larger than 0. We note that the equilibrium wind speeds should follow equation 2.24. When comparing a linear to a logarithmic grid we evaluate how it converts to this equilibrium solution.

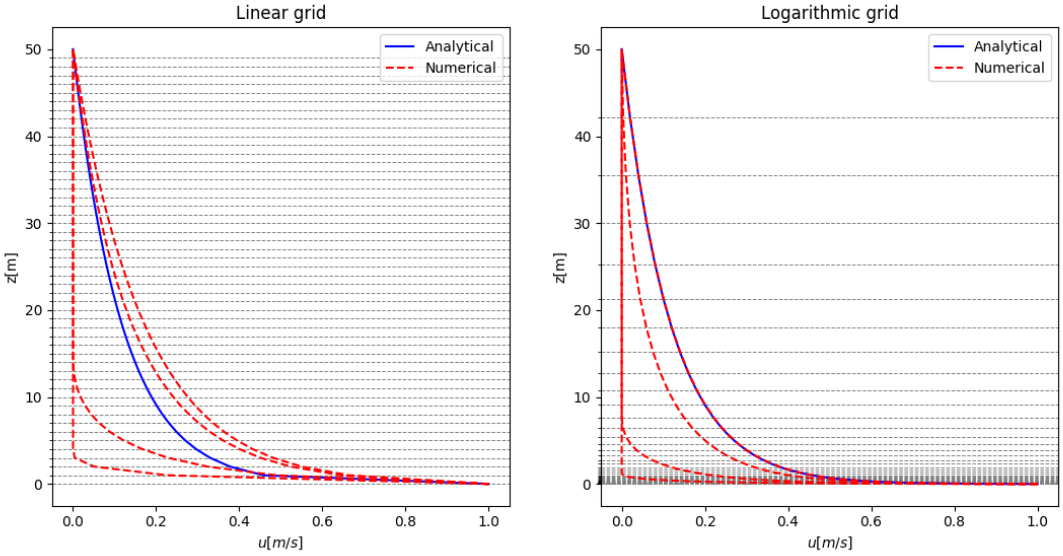

Figure 3.7: Turbulent wind speeds for constant velocity $u(z_0) = 1\frac{m}{s}$ with left a linear grid and right a log grid. The grid points are visualized by horizontal dashed gray lines. The solution is plotted for increasing t such that the solution moves to an equilibrium. For the logarithmic grid this solution converges to the analytical equilibrium solution in blue. For the linear plot it does not converge to the analytically computed equilibrium.

As we can see, the solution with a linear grid overshoots the solution whereas the logarithmic solution seems to exactly convert to the equilibrium position. Therefore it is believed that the logarithmic grid works better for turbulent flow so from now on we will use a logarithmic grid point distribution.

3.2.2 Boundary conditions taken from real measurements

For the data driven measurements we have taken the current speed at Buitenbanken West for 5 days[15]. We first simulated it for $u_{top} = 0$ at $z_{top} = 100m$. The last day is shown in the figure below.

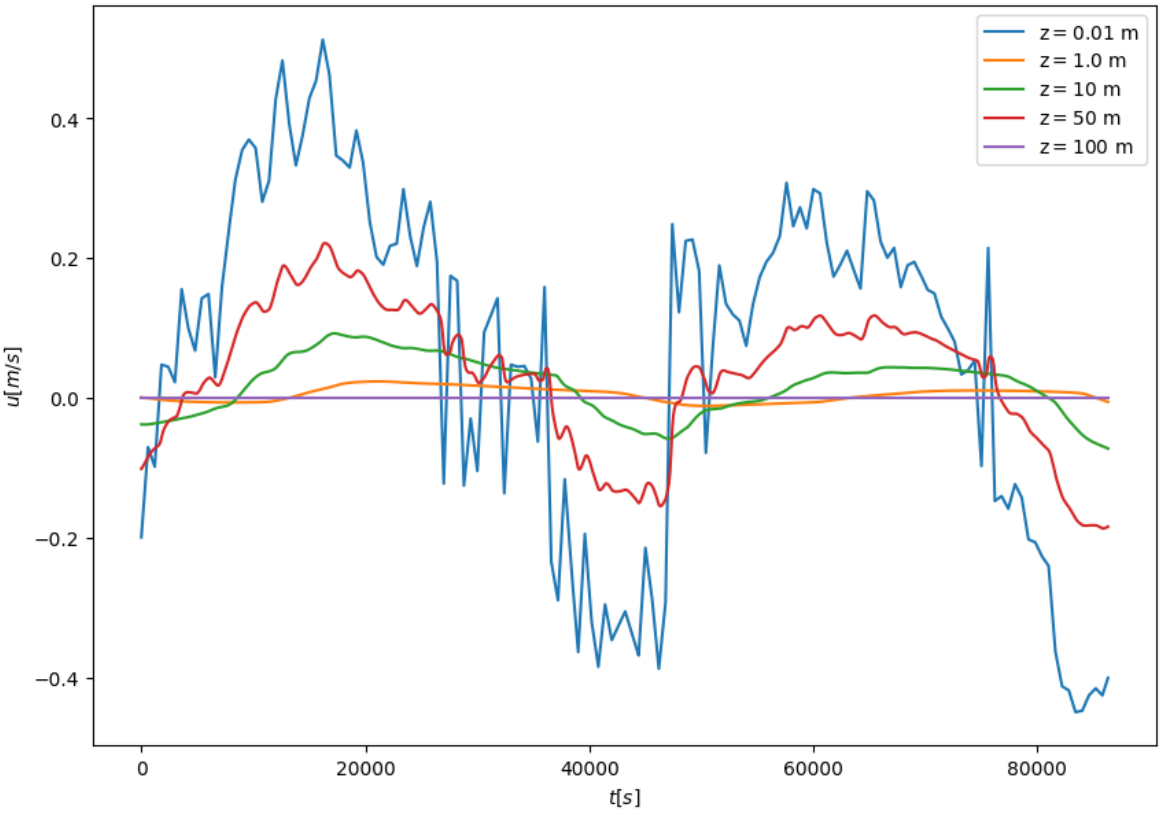

Figure 3.8: Simulated turbulent wind speeds plotted for the last day after 5 days for $z = 0.01, 1.0, 10, 50$ and $100m$. At $z = 10m$ the amplitude seems to be approximately $1/4$ of the tidal current amplitude. The boundary condition at $z = 0.01m$ is a measurement and the wind velocity at the $100m$ is set to $0\frac{m}{s}$. The values shown for $z = 1.0, 10$ and $50m$ are simulated with the numerical model.

In this simulation, the tidal wind at $z = 10m$ has an amplitude of one-fourth the amplitude of the boundary condition at the sea surface. At $z = 50m$ it can be seen that the influence of the bottom boundary condition is very small, approximately an amplitude of $1/20$ of the tidal current amplitude.

Using data from the Dutch Offshore Wind Atlas [10], it was found that the wind velocity at $100m$ was around $10\frac{m}{s}$ in amplitude and an approximate period of $1-2$ days. The wind is converted to only one direction, aligned with the surface current. We will simulate the same 5 days but then with a top boundary with amplitude $10\frac{m}{s}$ and a period of 1 day. Now we will evaluate the difference between two simulations with and without sea current velocity. So for the first simulation we use the measured sea current and for the second we set the current speed to 0, we plot the difference.

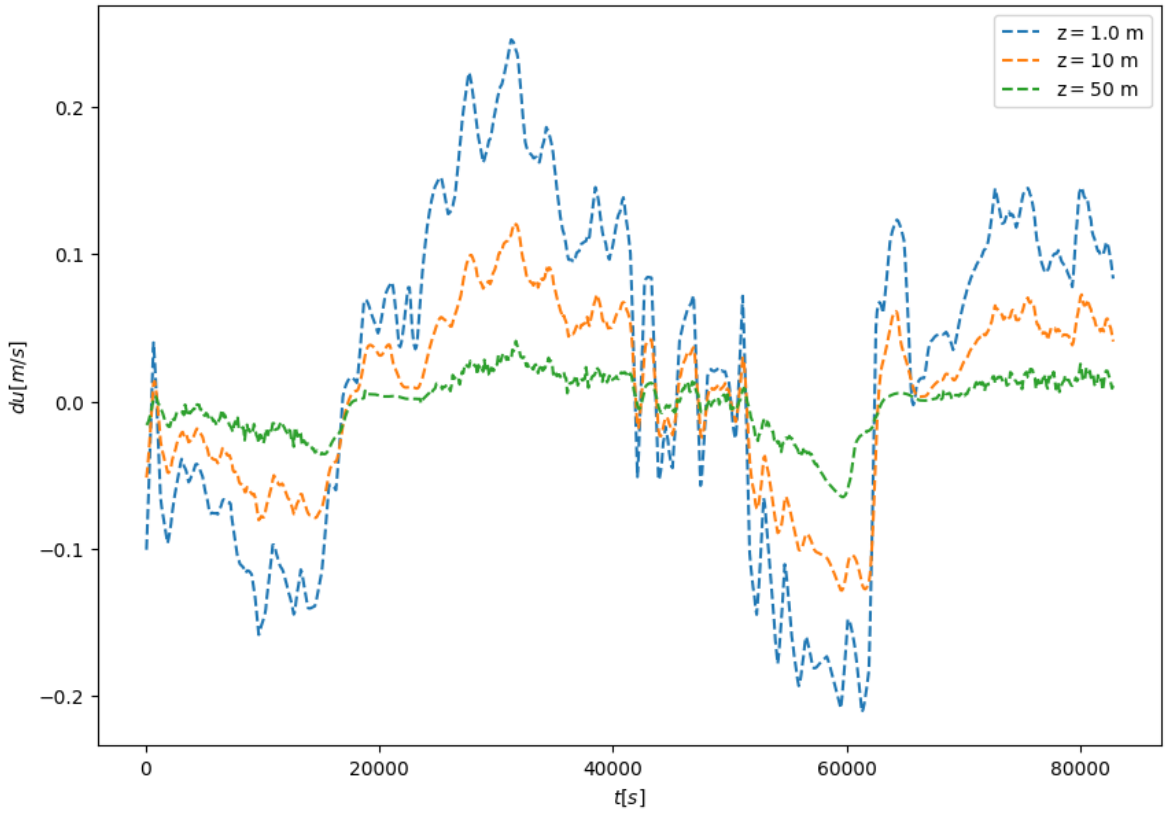

Figure 3.9: Simulated difference in turbulent wind speeds plotted for the last day after 5 days for $z = 1.0, 10$ and $50m$. The difference between a simulation with moving bottom boundary and velocity 0 as bottom boundary is plotted. The boundary condition at $z = 0.01m$ in the first simulation is again a measurement with an approximate amplitude of $0.4\frac{m}{s}$, in the second simulation it is $0\frac{m}{s}$. The top boundary at $z = 100m$ is now a periodic velocity with amplitude $10\frac{m}{s}$ and a period of 1 day. The approximate amplitude at $10m$ is $0.13\frac{m}{s}$ and at $50m$ the amplitude is approximately $0.03\frac{m}{s}$.

We would expect that with higher wind speeds and thus a higher velocity gradient, we would have a larger influence of the tidal currents, due to the dependence on the gradient. However, at $z = 10m$ it can be seen that the amplitude difference is still one-fourth of the tidal current amplitude. For $z = 50m$ it is around one-sixteenth.

Discussion

We have to note that in our study we made a lot of assumptions. Turbulent flow is very hard to model, especially when in our case we wanted to keep it very simple. The mixing length model is a relatively simple model compared to other turbulence models[8]. By the creator itself, Prandtl, it was called "only a rough approximation"[2]. However in a lot of boundary layer problems it does work surprisingly well. The mixing length hypothesis is conceptually analogous to the concept of mean free path in thermodynamics. A fluid parcel will travel a characteristic length before mixing with the surrounding fluid and losing it's original properties. However for this to work in the atmospheric boundary layer, the boundary layer needs to be neutrally stratified. Although this can happen, the atmosphere is very chaotic and certainly not always neutrally stratified. Buoyancy effects and pressure gradients most of the time play a large role in the atmospheric boundary layer as well. Furthermore, the influence of solar heating and latent heat was neglected.
When we look at the error measurement that was done for the laminar case with a periodic velocity at the bottom boundary, we see that the error scales quadratically with the time step as expected. However, the error did not significantly decrease for different grid sizes. This was most probably due to the fact that it was limited by the time step error. If we had more computing power or time, it would have been interesting to use even smaller time steps. In the error measurement, the tolerances were set really high such that they did not have an influence. In the actual simulations they were set to $atol = 10^{-4}$ and $rtol = 10^{-5}$ but this only had a positive effect on the error, the error decreased.
The biggest assumption comes from assuming that the wind and the current are in the same direction. In the data used from measurements, the wind was converted to only one direction. In reality this is not the case most of the times. The wind at lower heights may be mostly horizontal but it is certainly not limited to one direction. Therefore, the most logical next step for this model would be to expand it such that you consider two horizontal wind directions u and v. This way we can account for the angle the wind direction and the surface current make. Furthermore, the maximum height could be increased such that the solution can be determined for larger heights than $100m$. This does however add new complexities such as the Coriolis force.

Conclusion

In this report we investigated the influence of tidal currents on wind speeds above the coast of the Netherlands. For this purpose a numerical model was developed based on the 1-D Navier-Stokes equations in combination with the mixing length turbulence model, to solve for the horizontal wind speeds in a vertical grid with boundary condition at the bottom, the sea surface, and the top of the surface layer. The model was first validated with laminar flow using analytically computed solutions. Then it was used for turbulent flow to model the actual behaviour of the atmosphere above the coast. In the result it was found that tidal currents do have an influence on overlying wind patterns. At a height of $z = 10m$ above the sea level the amplitude of the wind speed that was induced by the velocity of the water surface was approximately one-fourth of the underlying tidal current. For $z = 50m$ it was already only $1/20$ for the simulation without wind and $1/16$ for the simulation with top boundary wind velocity. As wind farms are typically a couple hundred meters tall, the effect tidal winds will have on them will be very small according to this result. A factor of one-fourth at $10m$ is reasonably close to the found one-third in the English Channel by Renault and Marchesiello[13]. However if we look closely at our model, we have to realise that a lot of assumptions were made. A lot of boundary layer effects such as surface heating, latent heat and waves at the sea surface were ignored. Moreover, the wind velocity and tidal current direction were assumed to be aligned in the same direction. In reality this is of course almost never entirely true. Therefore, in order to improve on the model, the addition of a second wind velocity could be considered such that all horizontal winds can be simulated. This way you can account for the different angles between the wind and the tidal currents. Furthermore, we have only simulated up to $100m$, in order to expand the top boundary could be increased to for example $500m$ or even more. This would add a lot of complexity though, because at higher altitudes different effects come in to play such as the Coriolis effect.

Bibliography

[1] H. van den Akker en Rob Mudde. "Fysische Transportverschijnselen - denken in balansen". In: De Gruyter, 2023. Chap. 3. ISBN: 978-90-6562-4055.

[2] P. Bradshaw. "Possible origin of Prandtl's mixing-length theory". In: *Nature* 249 (1974), pp. 135–136.

[3] CBS. *Hernieuwbare elektriciteit; productie en vermogen*. 2019. URL: https://opendata.cbs.nl/statline/#/CBS/nl/dataset/82610NED/table?ts=1617545569760.

[4] D. B. Chelton, M. G. Schlax, and R. M. Samelson. "Summertime Coupling between Sea Surface Temperature and Wind Stress in the Californian Current System". In: *Journal of Physical Oceanography* 37.3 (2007), pp. 495–517.

[5] ECMWF. "IFS Documentation CY48R1 - Part IV: Physical Processes". In: 4. ECMWF, June 2023. DOI: 10.21957/02054f0fbf.

[6] D.-G. f. C. A. European Commission. *Going cimate-neutral by 2050 - A strategic long-term vision for a prosperous, modern, competitive and climate-neutral EU economy*. 2019. URL: https://data.europa.eu/doi/10.2834/02074.

[7] D. Government. *Planning windenergie op zee 2030 gereed*. June 2022. URL: https://www.rijksoverheid.nl/actueel/nieuws/2022/06/10/planning-windenergie-op-zee-2030-gereed.

[8] E. Hairer and G. Wanner. "Solving Ordinary Differential Equations II : Stiff and Differential - Algebraic Problems". In: Springer, 1991. Chap. 4.

[9] J. R. Holton and G. J. Hakim. "An Introduction to Boundary Layer Meteorology". In: 5th ed. Elsevier, 2013. Chap. 8. ISBN: 978-0-12-384866-6.

[10] R. N. M. Institute. *Dutch Offshore Wind Atlas - time series files for 2018 at 10-600 meter height at individual 2,5 km grid location*. URL: https://dataplatform.knmi.nl/dataset/dowa-netcdf-ts-singlepoint-upd-1 (visited on 07/13/2024).

[11] W. Lahoz, B. Khattatov, and R. Menard. *Data Assimilation: Making sense of observations*. 1st ed. Springer, 2010.

[12] L. Renault et al. "Modulation of Wind Work by Oceanic Current Interaction with the Atmosphere". In: *Journal of Physical Oceanography* 46.6 (2016), pp. 1685–1704.

[13] L. Renault and P. Marchesiello. "Ocean tides can drag the atmosphere and cause tidal winds over broad continental shelves". In: *Communications Earth & Environment* 3.70 (2022).

[14] L. Renault, J. C. McWilliams, and J. Gula. "Dampening of Submesoscale Currents by Air-Sea Stress Coupling in the Californian Upwelling System". In: *Scientific Reports* 8.13388 (2018).

[15] Rjkswaterstaat. *Rijkswaterstaat Waterinfo*. URL: https://waterinfo.rws.nl/#/thema/Waterbeheer (visited on 07/13/2024).

[16] W. Rodi. "Turbulence models and their applications in hydraulics". In: The Netherlands : International Association for Hydraulic Research, 1984. Chap. 2.

[17] D. Stammer. "Global Characteristics of Ocean Variability Estimated from Regional TOPEX/POSEIDON Altimeter Measurements". In: *Journal of Physical Oceanography* 27.8 (1997), pp. 1743–1769.

Appendix A

A.1 Analytical solutions

In this chapter we will elaborate on the analytical solutions given in the report

A.1.1 Laminar flow constant boundary

We start by restating our problem for the laminar problem with one constant boundary

$$\begin{aligned} u_t &= \nu u_{zz} \\ u(z_0, t) &= A \\ u(z_{top}, t) &= 0 \\ u(z, 0) &= 0 \end{aligned} \tag{A.1}$$

we will solve this using separation of variables starting by formulating a new $u' = u - A\frac{z_{top}-z}{z_{top}-z_0}$. This changes the problem to

$$\begin{aligned} u'_t &= \nu u'_{zz} \\ u'(z_0, t) &= 0 \\ u'(z_{top}, t) &= 0 \\ u'(z, 0) &= -A\frac{z_{top} - z}{z_{top} - z_0} \end{aligned} \tag{A.2}$$

performing separation of variables $u' = \phi(z)h(t)$ leads to

$$\frac{1}{\nu h}h_t = \frac{1}{\phi}\phi_{zz} = -\lambda \tag{A.3}$$

which gives a set of new ordinary differential equations

$$\begin{aligned} \phi_{zz} &= -\lambda\phi & \qquad h_t &= -\nu\lambda h \\ \phi(z_0) &= 0 & \qquad \phi(z)h(0) &= -A\frac{z_{top} - z}{z_{top} - z_0} \\ \phi(z_{top}) &= 0 \end{aligned}$$

Solving for ϕ gives $\phi_n = C_n sin(n\pi\frac{z-z_0}{z_{top}-z_0})$, so $\lambda_n = (\frac{n\pi}{z_{top}-z_0})^2$. Solving for h gives $h_n(t) = c_n e^{-\nu(\frac{n\pi}{z_{top}-z_0})^2 t}$. This results in

$$u'(z, t) = \sum_{n=1}^{\infty} C_n sin(n\pi\frac{z - z_0}{z_{top} - z_0})e^{-\nu(\frac{n\pi}{z_{top}-z_0})^2 t} \tag{A.4}$$

From the initial condition we get

$$
\begin{aligned}
C_n &= \frac{\int_{z_0}^{z_{top}} -A\frac{z_{top}-z}{z_{top}-z_0} sin(n\pi\frac{z-z_0}{z_{top}-z_0})\,dz}{\int_{z_0}^{z_{top}} sin(n\pi\frac{z-z_0}{z_{top}-z_0})^2\,dz} \\
C_n &= -\frac{2A}{z_{top}-z_0}\int_{z_0}^{z_{top}} \frac{z_{top}-z}{z_{top}-z_0} sin(n\pi\frac{z-z_0}{z_{top}-z_0})\,dz \\
C_n &= -\frac{2A}{z_{top}-z_0}\frac{z_{top}-z_0}{n\pi} \\
C_n &= -\frac{2A}{n\pi}
\end{aligned}
\tag{A.5}
$$

So we get u' and thus also u

$$
\begin{aligned}
u'(z,t) &= -\sum_{n=1}^{\infty}\frac{2A}{n\pi} sin(n\pi\frac{z-z_0}{z_{top}-z_0}) e^{-\nu(\frac{n\pi}{z_{top}-z_0})^2 t} \\
u(z,t) &= A\frac{z_{top}-z}{z_{top}-z_0} - \sum_{n=1}^{\infty}\frac{2A}{n\pi} sin(n\pi\frac{z-z_0}{z_{top}-z_0}) e^{-\nu(\frac{n\pi}{z_{top}-z_0})^2 t}
\end{aligned}
\tag{A.6}
$$

A.1.2 Laminar flow periodic boundary

We start again by restating the problem

$$
\begin{aligned}
u_t &= \nu u_{zz} \\
u(z_0,t) &= Acos(\omega t) \\
u(z_{top},t) &= 0 \\
u(z,0) &= f(z)
\end{aligned}
\tag{A.7}
$$

we note that we expect the solution to be independent of the initial condition for $t \to \infty$, so

$$
u(z,t) = v(z,t) + u_{qss}(z,t) \tag{A.8}
$$

where $v(z,t) \to 0$ for $t \to \infty$ is due to the initial condition and $u_{qss}(z,t) = A(z)cos(\omega t + \phi(z))$ is the quasi-steady state solution. Note that if we take $f(z) = u_{qss}(z,0)$ we don't have to look at the initial condition at all. We will now solve for u_{qss}. First we will start to use complex exponentials, as they are easier to work with

$$
\begin{aligned}
u_{qss}(z,t) &= A(z)cos(\omega t + \phi(z)) \\
u_{qss}(z,t) &= Re\{A(z)e^{i\phi(z)}e^{i\omega t}\} \\
u_{qss}(z,t) &= Re\{U(z)e^{i\omega t}\} \\
u_{qss}(z,t) &= \frac{1}{2}(U(z)e^{i\omega t} + U^*(z)e^{-i\omega t})
\end{aligned}
\tag{A.9}
$$

substituting in the partial differential equation gives

$$
\begin{aligned}
\frac{i\omega}{2}(U(z)e^{i\omega t} - U^*(z)e^{-i\omega t}) &= \nu\frac{1}{2}(U_{zz}(z)e^{i\omega t} + U^*_{zz}(z)e^{-i\omega t}) \\
(i\omega U(z) - \nu U_{zz}(z))e^{i\omega t} - (i\omega U^*(z) + \nu U^*_{zz}(z))e^{-i\omega t} &= 0 \\
i\omega U(z) - \nu U_{zz}(z) &= 0 \\
U_{zz}(z) &= \frac{i\omega}{\nu}U(z)
\end{aligned}
\tag{A.10}
$$

where we used that if $ae^{i\omega t} + be^{-i\omega t} = 0$ for all $t > 0$, then $a = b = 0$ (*Hier nog bron*). Substituting A.9 into the boundary conditions gives

$$\frac{1}{2}(U(z_0)e^{i\omega t} + U^*(z_0)e^{-i\omega t}) = \frac{A}{2}(e^{i\omega t} + e^{-i\omega t}), \qquad \frac{1}{2}(U(z_{top})e^{i\omega t} + U^*(z_{top})e^{-i\omega t}) = 0 \tag{A.11}$$

$$(U(z_0) - A)e^{i\omega t} + (U^*(z_0) - A)e^{-i\omega t} = 0, \tag{A.12}$$

$$U(z_0) = A, \qquad U(z_{top}) = 0 \tag{A.13}$$

where we again used $a = b = 0$ if $ae^{i\omega t} + be^{-i\omega t} = 0$ for $t > 0$.
Now we have an ordinary differential equation for U. Note that $\frac{i\omega}{\nu} = (\sqrt{\frac{\omega}{2\nu}}(1+i))^2$. Solving the ordinary differential equation gives

$$U(z) = c_1 cos(\sqrt{\frac{\omega}{2\nu}}(1+i)(z_{top} - z)) + c_2 sin(\sqrt{\frac{\omega}{2\nu}}(1+i)(z_{top} - z)) \tag{A.14}$$

using A.13 we get $c_1 = 0$ and $c_2 = Acsc(\sqrt{\frac{\omega}{2\nu}}(1+i)(z_{top} - z_0))$, where $csc(x) = \frac{1}{sin(x)}$ is the cosecant function. Substituting the equation for $U(z)$ in equation A.9, we get

$$u_{qss}(z,t) = \frac{A}{2}(\frac{sin(\sqrt{\frac{\omega}{2\nu}}(1+i)(z_{top} - z))}{sin(\sqrt{\frac{\omega}{2\nu}}(1+i)(z_{top} - z_0))}e^{i\omega t} + \frac{sinh(\sqrt{\frac{\omega}{2\nu}}(1+i)(z_{top} - z))}{sinh(\sqrt{\frac{\omega}{2\nu}}(1+i)(z_{top} - z_0))}e^{-i\omega t}) \tag{A.15}$$

where we used that $sin(\alpha(1+i))^* = sinh(\alpha(1+i))$ with α real.

A.1.3 Turbulent flow constant boundary

We start by restating the problem

$$\begin{aligned} u_t &= \frac{\partial}{\partial z}[(\nu + \kappa^2 z^2 |u_z|)u_z] \\ u(z_0, t) &= A \\ u(z_{top}, t) &= 0 \\ u(z, 0) &= 0 \end{aligned} \tag{A.16}$$

we are only looking for a steady state solution, so $u_t = 0$ and we do not have to look at the initial condition. Because we are considering the solution from z_0, which is slightly above the actual sea surface at 0, we can neglect the influence of the dynamic viscosity ν which only plays a large role right at the boundary layer near $z = 0$, so

$$\begin{aligned} 0 &\approx \frac{\partial}{\partial z}[(\kappa^2 z^2 |u_z|)u_z] \\ \kappa^2 z^2 |u_z| u_z &= C^2 \\ u_z &= \frac{C}{\kappa z} \\ u &= C_1 log(\frac{z}{C_2}) \end{aligned} \tag{A.17}$$

with C, C_1, C_2 arbitrary constants. If we now implement the boundary conditions we can see that $C_2 = z_{top}$ such that $u(z_{top}) = 0$. By the boundary condition at z_0 we can determine C_1 which gives us as a steady state profile

$$u_{ss}(z) = A\frac{log(\frac{z}{z_{top}})}{log(\frac{z_0}{z_{top}})} \tag{A.18}$$